4-Sulfonatocalixarene-induced nanoparticle formation of methylimidazolium-conjugated dextrans: Utilization for drug encapsulation

Véronique Wintgens,[a] Jean-Michel Guigner,[b] Zsombor Miskolczy,[b] Catherine Amiel,[a] László Biczók[b,*]

[a]*Université Paris Est, ICMPE (UMR7182), CNRS, UPEC, F 94320 Thiais, France*

[b]*Institut de Minéralogie, de Physique des Matériaux et de Cosmochimie, IMPMC, Sorbonne Université, IRD, CNRS UMR 7590, MNHN,4 Place Jussieu, 75005 Paris, France*

[c]*Institute of Materials and Environmental Chemistry, Research Centre for Natural Sciences, Hungarian Academy of Sciences, P.O. Box 286, 1519 Budapest, Hungary*

[*] Corresponding author. Phone: (+36 1) 382-6614; E-mail: biczok.laszlo@ttk.mta.hu

Abstract

Methylimidazolium side groups were grafted via ether linkage to dextran and the self-assembly of these polymers with 4-sulfonato-calix[n]arenes (SCXn) was studied in aqueous solutions. Dynamic light scattering and zeta potential measurements revealed the mixing ratio ranges of the constituents where stable nanoparticles could be created. The macrocycle size of SCXn and the molecular mass of the polymer barely affected the nanoparticle diameter, but the lowering of the imidazolium degree of substitution substantially diminished the stability of the associates. The pH change from neutral to acidic also unfavourably influenced the self-organization owing mainly to the decrease of the SCXn charge. Cryogenic transmission electron microscopy images proved the spherical morphology of the nanoproducts in which the stoichiometry of the constituents was always close to the one corresponding to charge compensation. The flexible and positively charged dextran-chains are compacted by the polyanionic SCXn. Coralyne, a pharmacologically important alkaloid was efficiently embedded by self-assembly in the produced nanoparticles reaching 99 % association efficiency.

Key words

cationic polymer, macrocycle, self-assembly, alkaloid, drug delivery

1. Introduction

The self-assembly of naturally occurring biocompatible and biodegradable polysaccharides and their derivatives have attracted rapidly growing interest (Giri & Ghosh, 2018; Myrick James, Vendra Venkat & Krishnan, 2014; Zheng, Monty & Linhardt, 2015). Dextrans, the glucose polymers of microbial origin, represent a particularly important family of these substances because of their diverse biomedical applications (Heinze, Liebert, Heublein & Hornig, 2006; Maia, Evangelista, Gil & Ferreira, 2014). Their favorable properties offer great potential for the delivery and controlled release of drugs (Huang & Huang, 2018; Mehvar, 2000). Chemical modification of the polymer backbone created conjugates capable of the encapsulation of various compounds via self-organization into stimuli-responsive nanoparticles (Jafarzadeh-Holagh, Hashemi-Najafabadi, Shaki & Vasheghani-Farahani, 2018; Son et al., 2018; Tang et al., 2018). The introduction of spermin, histidine, or diethylaminoethyl units led to polycations usable for gene delivery (Hosseinkhani, Azzam, Tabata & Domb, 2004; Pawar et al., 2008; Thomas, Rekha & Sharma, 2012). Improved DNA carrier ability was achieved by grafting of dextran onto branched polyethylenimine (Tseng & Jong, 2003). The association with dextran sulfate was exploited to enhance the bioavailability of poorly-soluble cationic drugs (Cheow & Hadinoto, 2012; Megyesi, Biczók & Görner, 2009; Persson, Hugerth, Caram-Lelham & Sundelöf, 2000). A dextran-based prodrug produced micelles from which the pharmaceutically active component was liberated by the hydrolysis at the acidic endosomal pH (Jin, Guo, Dong, Xie & Cao, 2017). The monofunctionalized derivative labelled with a fluorogenic probe exhibited improved cellular imaging capabilities and was efficiently transported into the cytosol (Chyan, Kilgore & Raines, 2018). Dextrans with pendant side chains bearing quaternary ammonium group were synthesized and their aggregation was extensively studied (Bai, Nichifor, Lopes & Bastos, 2005; Nichifor, Lopes, Bastos & Lopes, 2004; Nichifor, Stanciu & Simionescu, 2010; (Prado

& Matulewicz, 2014). However, much less information is available on the derivatives carrying methylimidazolium substituents. These biodegradable polymers can serve as flocculants in the separation of contaminants of wastewater (Ghimici & Nichifor, 2018).

We have previously shown that 1-alkyl-3-methylimidazolium cations readily bind to 4-sulfonatocalixarenes (SCXn) (Wintgens, Biczók & Miskolczy, 2011) and the formed inclusion complexes self-assemble into nanoparticles (NP) or supramolecular micelles (Wintgens et al., 2013) if the number of carbon atoms in the aliphatic substituent of the heterocycle is at least 12. More stable and less toxic NPs may form with SCXn when methylimidazolium groups are connected to polymer chain by covalent bonds. The interior of such species can provide protective matrix for pharmaceutical agents ensuring longer duration of action by sustained release. The confinement in NPs may enhance the bioavailability of poorly soluble therapeutics. The utilization of dextrans is expected to be beneficial because of their good water solubility and biocompatibility. The strengthening of the interaction with SCXn polyanionic macrocycles can be achieved by grafting of cationic substituents to the dextran main chain. Despite the importance of the polymer-based NPs, few information has been gathered so far on the SCXn-induced noncovalent crosslinking of macromolecules and on the properties of the nanostructures created thereby. It is unknown how the competitive binding of the pendant moieties to SCXn affects the incorporation of drugs.

In the present study, we focus on the association of methylimidazolium-conjugated dextrans with SCXn to reveal how the degree of substitution (DS) of the polymer affects the characteristics of the produced aggregates. Our other goal is to compare the drug loading capability of the created nanoparticles with those previously synthetized from protonated chitosan and SCXn (Harangozó, Wintgens, Miskolczy, Amiel & Biczók, 2016). We linked methylimidazolium cationic groups to dextran because these are very weak acids and cannot

be protonated. Hence, the produced polymer can be used in a wide pH range in contrast with protonated chitosan-SCXn associates, which were applicable only in acidic medium. Coralyne, a synthetic analogue of natural protoberberine alkaloids, was used as a model compound because it shows high affinity and multiple binding to SCXn. (Megyesi & Biczók, 2010) Coralyne exhibited antitumor activity (Gatto et al., 1996; Kumari, Badana, Mohan, Shailender Naik & Malla, 2017) and was successfully employed in the phototherapy of cancer (Bhattacharyya, Gupta, Bandyopadhyay, Patro & Chattopadhyay, 2018; Bhattacharyya, Saha, Tyagi, Bandyopadhyay, Patro & Chattopadhyay, 2017). The chemical structures of the investigated compounds are displayed in Scheme 1.

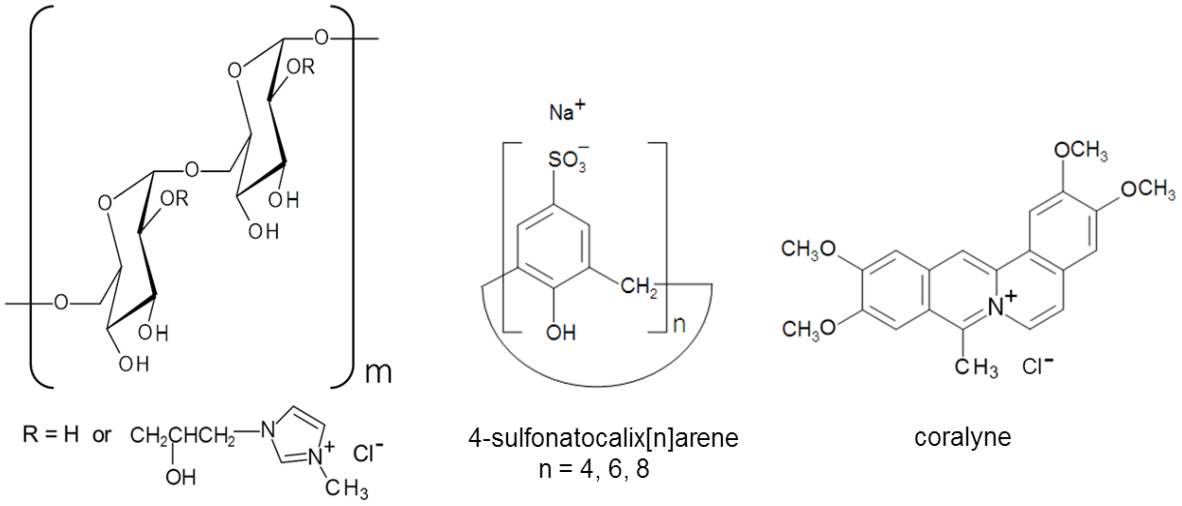

Scheme 1. Formulas of the studied compounds

2. Materials and method

2.1. Materials.

4-Sulfonatocalix[n]arenes (SCX4, SCX6 and SCX8) were purchased from Acros Organics and used after being dried under vacuum at 343 K overnight. Double distilled water served as solvent. Dextrans with molar mass of 40 (D40), 70 (D70), 110 (D110) and 500 (D500) kg mol^{-1} were purchased from Amersham Pharmacia (Sweden) and used as received.

These samples had a branching ratio below 5% according to the specifications of the manufacturer. 1-Methylimidazole (Acros) and epichlorohydrin (Aldrich) were also employed without further purification. The modified polymers were studied after being dried under vacuum at 343 K overnight. Coralyne chloride (Acros Organics) was recrystallized from ethanol.

2.2. Synthesis of the chemically modified dextrans.

The various modified dextrans were synthesized as reported by Nichifor and coworkers (Nichifor, Stanciu & Simionescu, 2010). In this one-step procedure, typically 1g dextran (6.17 mM anhydroglucose units, AGU) was dissolved in 10 mL water. Then, 2.7 mL 1-methylimidazole (33.9 mM) and 2.2 mL epichlorohydrin (27.8 mM) were added, which corresponded to a molar excess (versus AGU) of 5.5 and 4.5 for the former and latter compounds, respectively. The mixture was stirred for 24 hours at 313 K. After cooling, the mixture was set in a dialysis bag (6000-8000 Da molecular weight cut off). Two dialyses against 0.1 M HCl and eight dialyses against water were performed. The final product (~0.8 g) was obtained after lyophilization. Following this procedure, three dextran derivatives were prepared with slightly different degrees of substitution: D40Im46, D70Im54, D110Im43, where *x* and *y* in D*x*Im*y* stand for the starting dextran molar mass (kg mol^{-1}) and the % of imidazolium groups, respectively. The latter quantity, expressed as the number of imidazolium substituents per 100 AGU, was obtained by ^{1}H NMR spectroscopic measurements in D_2O in the presence of deuterated trifluoroacetic acid as reported in the Supplementary data. In the case of dextrans possessing the highest molecular weight (D500), the synthesis led to gelation. To avoid this, the synthesis was carried out in 25 mL water and a modified dextran with a lower substitution degree was isolated (D500Im25). To enhance the substitution degree, five times higher amounts of each reactants were used in 60 mL water and D500Im44 was obtained. A dextran with the lowest molecular weight and with an

imidazolium DS around 0.22 (D40Im22) was also prepared in 10 mL water using twice less amount of 1-methylimidazole and epichlorohydrin than described above.

2.3. Nanoparticle preparation

Stock solutions of the dextrans were prepared at least one day before the start of the experiments. The pH of SCXn in water was adjusted to 7 by addition of concentrated NaOH solution. Nanoparticles (NPs) were prepared by mixing appropriate amounts of dextran derivative (5 g L^{-1}) and SCXn (2 mM) solutions in various molar ratios at 276 K under stirring at 150 rpm. Coralyne (Cor) loaded NPs were created using a Cor–SCX8 mixture instead of SCX8.

2.4. Instrumentation

^{1}H NMR spectra were recorded in D_2O in presence of in presence of few drops (~50 µL in 1mL solution) of deuterated trifluoroacetic acid on a Bruker Avance II 400 MHz NMR spectrometer. The absorption spectra were taken on an Agilent Technologies Cary60 spectrophotometer. Size exclusion chromatography was performed on a chromatograph equipped with a pump P 100 (Spectra-Physics, Fremont, CA, USA). A set of two columns PL-aquagel OH-30 and OH-40 (Polymer Laboratories, Shropshire, UK) was used for the analysis of polymers in aqueous 0.1 M $LiNO_3$ eluent. Two detectors were connected in series at the end of the columns: a Dawn Optilab Rex differential refractometer and a Dawn Heleos 8 light scattering detector (Wyatt Technology, Santa Barbara, CA, USA). The chromatographic analysis of polymers was done with polymer solutions at a concentration of 10 mg mL^{-1}. Particle size was determined by dynamic light scattering on a Zetasizer Nano-ZS (Malvern Instrument) equipped with a He-Ne laser (λ = 633 nm, scattering angle 173°) after stabilization at 296 K. Each measurement was the average of 14 runs of 10 seconds. The reported mean diameter (Z-average size) and polydispersity index (PDI) are obtained by

cumulant analysis (fit of the logarithm of the correlation function by a 3rd order polynomial). Error limit of ± 10 % was estimated for the Z-average size determination. NPs were separated from the liquid phase by an ultracentrifuge from Beckman Coulter (Optima Max-XP, type TLA 110 rotor). Total carbon analyses were performed on a Shimadzu TOC-L CSN instrument, which was calibrated by a potassium hydrogen phthalate solution in ultrapure water (2.125 g L^{-1} corresponding to 1000 mgC L^{-1}). Cryo-TEM images were taken on an Ultrascan 2 k CCD camera (Gatan, USA), using a LaB_6 JEOL JEM 2100 (JEOL, Japan) cryo-microscope operating at 200 kV with a JEOL low dose system (Minimum Dose System, MDS) to protect the thin ice film from any irradiation before imaging and to reduce the irradiation during the image capture. The images were recorded at 93 K and digitally corrected using the ImageJ software. The samples were prepared as previously described (Wintgens et al., 2013).

3. Results and discussion

3.1. Polymers

Methylimidazolium substituents were grafted via ether bond to dextran. Synthesis was a one-step procedure in water using epichlorohydrin and 1-methylimidazole as reactants (Nichifor, Stanciu & Simionescu, 2010). The modified dextrans were characterized by ^{1}H NMR (Figure S1) and the degree of substitution (DS) of the imidazolium moieties is given in Table 1. Four of the prepared polymers with an imidazolium DS around 47% (D40Im46, D70Im54, D110Im43, and D500Im44) were selected to monitor the effect of the molar mass variation from 40 kg mol^{-1} to 500 kg mol^{-1} keeping the imidazolium DS almost constant. We intended to compare the behavior of these polymers with those having an imidazolium DS around 24% (D40Im22 and D500Im25).

Table 1. Characteristics of the modified dextrans

	D40Im22	D40Im46	D70Im54	D110Im43	D500Im25	D500Im44
Dextran molar mass[a] ($g\ mol^{-1}$)	40 000	40 000	70 000	110 000	500 000	500 000
Imidazolium DS	0.22	0.46	0.54	0.43	0.25	0.44

[a] molar mass of the starting polymer

3.2. Characterization of nanoparticles

Charge ratio effect. As shown in Figure S2A, Tyndall effect was observed for different mixing ratios when SCXn was added to 1 g L^{-1} D70Im54 solution. This indicated NPs formation. NPs size was determined by dynamic light scattering (DLS). Representative examples for correlogram and DLS distribution are given in Figure S3. Figure 1 displays the

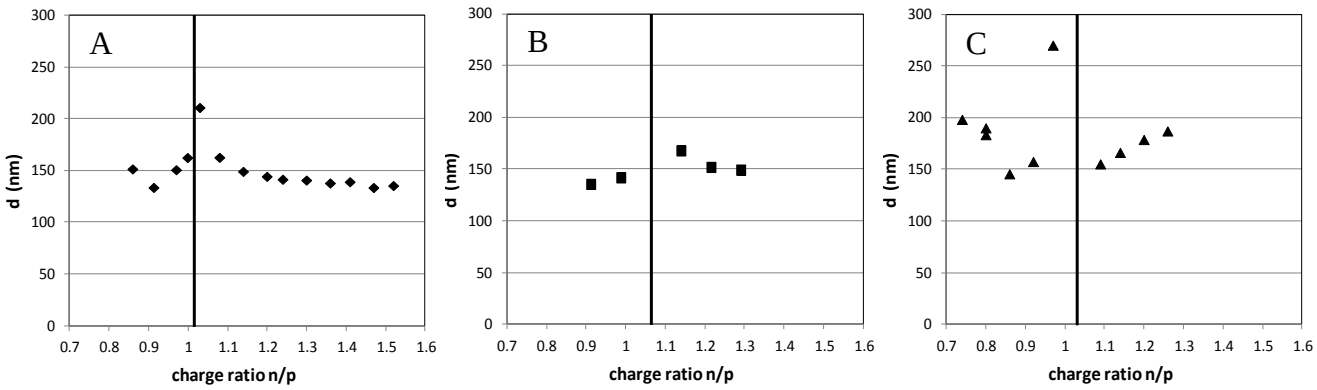

Figure 1. Particle diameter as a function of the mixing charge ratio n/p in the case of SCX4 (A), SCX6 (B) and SCX8 (C) at 1 g L^{-1} D70Im54 concentration and pH 7. On the left of the vertical lines NPs were positively charged.

alteration of NP diameters as a function of the negative/positive charge ratios (n/p) in the mixed SCXn and D70Im54 components. The data were plotted only for those NPs whose size remained almost unchanged over two hours. When the relative amount of SCXn was gradually raised keeping the polymer quantity constant, fast coalescence was found at n/p close to 1. At ratios below this coalescence point, NPs had a positive zeta potential (around +

22 mV), and reversely, above this point, they had a negative zeta potential (around -23 mV). Outside the vicinity of the coalescence region, NPs had ~150 nm ± 15 nm average diameter. Diameter, PDI and zeta potential values are given for several NPs in Table S2. The macrocycle size barely influenced the NP diameters, but altered the mixing range in which NPs were produced. The largest mixing range was obtained with SCX4 and even a large excess of SCX4 did not destabilize the NPs. The dextran molecular mass exerted a slight effect on the NPs size (Figure S4). The increase of the dextran molecular weight did not improve formation and stability of the NPs. Therefore, further studies were mainly performed with D70Im54 whose highest degree of substitution facilitated the formation of stable NPs.

Imidazolium DS effect. The SCXn-induced NP formation was sensitive to the diminution of the imidazolium DS. D40Im22 constituted negatively charged NPs stable for at least two hours only with the largest macrocycle SCX8 at a mixing charge ratio n/p of ~0.84. The NPs diameter was ~400 nm, much larger than that obtained with D40Im46 (~150 nm). D500Im25 and SCX4 self-organized at mixing charge ratio 1.04 into stable negatively charged NPs whose diameter was ~200 nm but unstable NPs emerged with SCX6. On the other hand, both positively and negatively charged stable NPs of ~170 nm diameter were prepared with D500Im25 and the largest SCX8 cavitand in a narrow range of mixing charge ratios.

NPs formation and stability depend on the number and density of links that can be established between the modified dextrans and SCXn. As the lessening of the substitution level diminishes the number and density of links, NPs formation is disfavored. Increasing the dextran molecular weight increases the number of links per chain, but this increase could not compensate the stability loss owing to the too low imidazolium DS in the case of D500Im25.

Effect of pH alteration. Without any pH adjustment, D70Im54–SCXn mixtures were acidic exhibiting slightly lower pHs than the negative logarithm of the equilibrium constants of the first phenolic OH deprotonation (pK_{a1} = 3.2, 2.7 and 3.0 for SCX4, SCX6 and SCX8,

respectively) (Suga, Ohzono, Negishi, Deuchi & Morita, 1998). Hence, SCXn macrocycles had less negative charges than at pH 7 where not only the sulfonic acid moieties but also one (SCX4 and SCX6) or two (SCX8) phenolic OH group(s) were deprotonated. Figure 2 presents the NPs diameters as a function of mixing charge ratios n/p. The zeta potential of NPs changed from positive to negative at mixing n/p close to 1, but this corresponds to higher SCXn concentrations than those found at pH 7: for example, 0.478 mM and 0.392 mM for

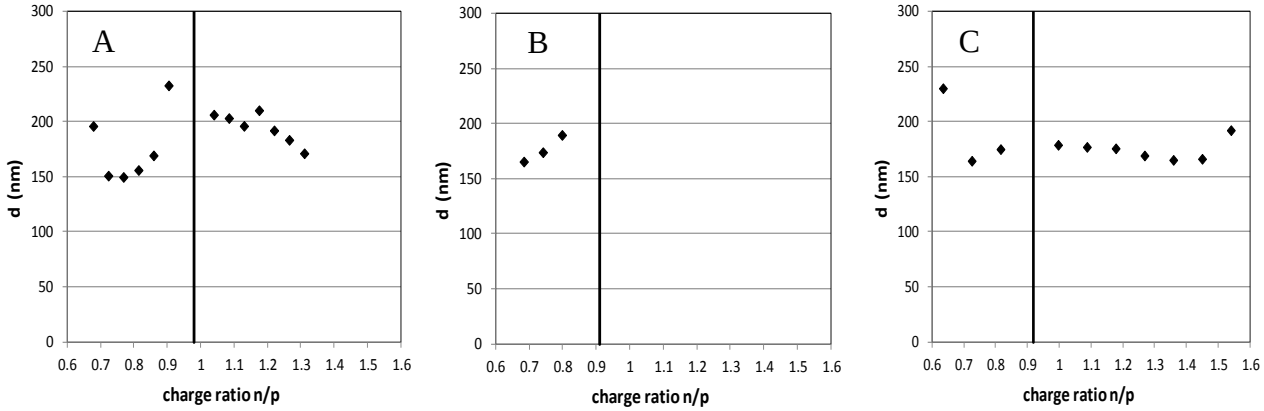

Figure 2. Particle diameter as a function of the mixing charge ratio n/p in the case of SCX4 (A), SCX6 (B) and SCX8 (C) at 1 g L^{-1} of D70Im54 without any pH adjustment (2 < pH < 3). On the left of the vertical line NPs were positively charged.

SCX4 in water and at pH 7, respectively. This is in accordance with the lower negative charge of SCX4 in acidic solution. Additionally, the mixing charge ratio range for NP formation and the stability of the associates were reduced for SCX4 and SCX6 under acidic conditions compared to those found in neutralized solutions. For instance, negatively charged NPs could not be created with SCX6 in acidic medium. Because of the more advantageous NP formation at pH 7, further studies were performed under such conditions.

Concentration effect. The rise of the modified dextran concentration brought about slight NP growth (Figure 3) and Tyndall effect enhancement (Figure S2B) in the presence of SCXn. The diameter increase with D70Im54 concentration depended on the mixing charge ratio. The

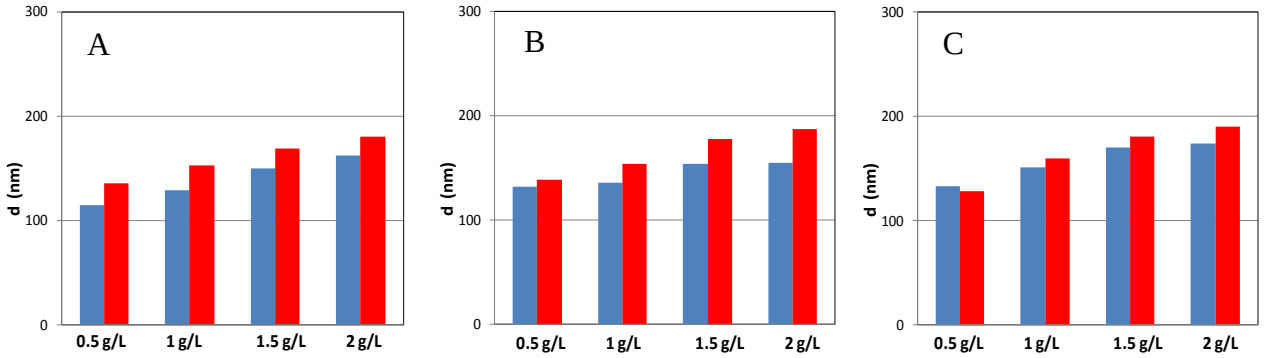

Figure 3. Particle diameter as a function of D70Im54 concentration (pH 7) with (A) SCX4 at mixing charge ratio n/p of 0.90 (■) and 1.19 (■); (B) SCX6 at mixing charge ratio n/p of 0.90 (■) and 1.20 (■); (C) SCX8 at mixing charge ratio n/p of 0.91 (■) and 1.13 (■).

closer this ratio was to that of charge compensation, the more significant diameter increase was found with polymer concentration. For example, at [D70Im54] = 2 g L^{-1}, the diameter of the negatively charged SCX4-containing NPs was 230 nm and 180 nm for mixing charge ratio of 1.07 and 1.19, respectively. Moreover, close to the charge compensation, the particles were less stable at larger polymer concentration. But even in more concentrated polymer solutions, wide mixing ratio ranges were found where both positively and negatively charged NPs did not change within more than one day. Figure S5 shows examples for the temporal stability of NPs.

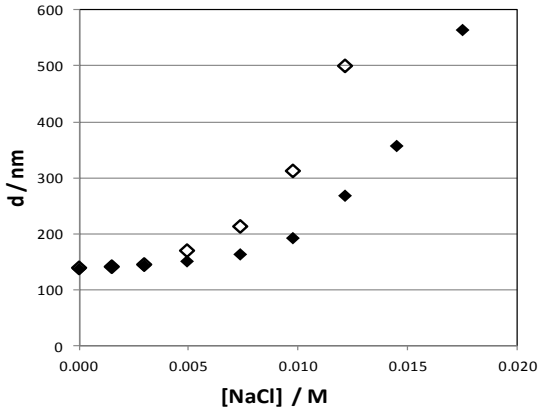

Figure 4. Variation of NP diameters as a function of NaCl concentration at pH 7. NPs were prepared from 1 g L^{-1} D70Im54 with SCX4 at mixing charge ratio n/p of 0.91 (◆) and 1.20 (◇)

Salt effect. Addition of NaCl to the NPs suspensions led to NPs destabilization for NaCl concentration larger than 8-10 mM (Figure 4). The charged NPs were mainly stabilized by electrostatic repulsions which were screened by salt addition. Same behavior was observed for other self-assembled nanoparticles made of adamantyl modified dextrans (Wintgens, Layre, Hourdet & Amiel, 2012).

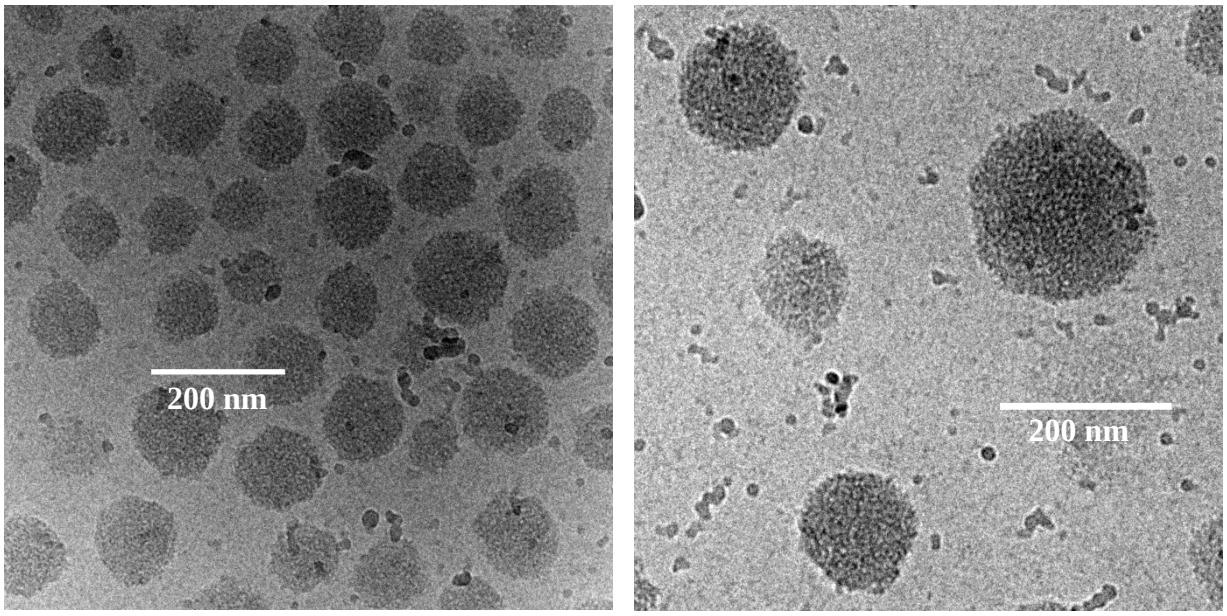

Figure 5. Cryo-TEM images of the NPs prepared from D70Im54 (2 g L^{-1}) with SCX4 at mixing charge ratio n/p of 0.91 at pH 7.

3.3. Morphology and composition of the nanoparticles.

Morphology. To get information about the shape and the internal structure of NPs, cryogenic transmission electron microscopy (cryo-TEM) images were recorded after mixing the components at 298 K. Figure 5 shows images for positively charged NPs composed of D70Im54 and SCX4 at pH 7. NPs were well-separated, spherical with a grainy appearance, or with small worm-like structures. In a few areas, NPs coalesced at the edge of the amorphous carbon film (Figure S6A), showing their affinity to the surface. The analysis of the cryo-TEM images of 190 NPs provided an average diameter of 112 ± 25 nm in good agreement with the results of DLS measurements. The negatively charged NPs formed from D70Im54 and SCX4

were less numerous on the grid, but had the same shape and appearance (Figure S6B). An average diameter of 151 ± 55 nm was determined, also in accord with the DLS data. The NPs formed from D70Im54 and SCX8 led to very similar images (Figure S7).

Composition. At the coalescence mixing ratio, the D70Im54–SCXn particles could be easily filtered and spectrophotometric measurements of the supernatant showed that on average more than 92% of SCXn was incorporated in NPs. Detailed studies were performed using SCX4 to get more information about the composition and formation efficiency of NPs. The suspensions obtained at various mixing ratios were ultra-centrifuged. The amount of SCX4 was monitored by spectrophotometry measuring the absorbance of both the SCX4 mother solution and the supernatant at 284 nm. From these absorbances, SCX4 concentrations were obtained in the supernatant and in the NPs (Wintgens et al., 2013). The total organic carbon analysis of the supernatant provided the sum of its SCX4 and D70Im54 concentrations. On the basis of this quantity and the spectrophotometrically determined SCX4 concentrations, the D70Im54 concentrations in the supernatant and in the NPs could be deduced.

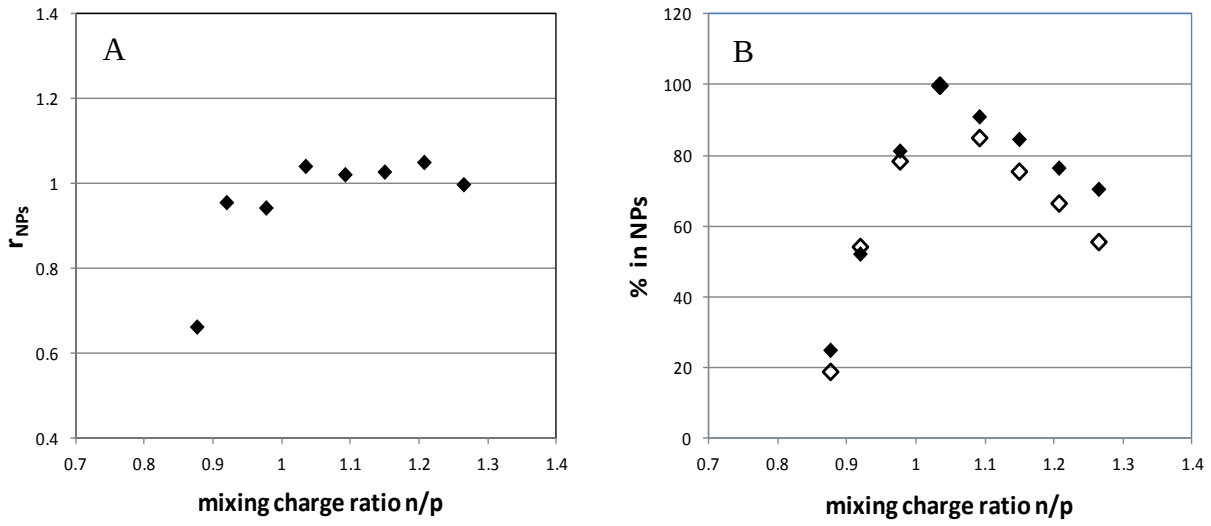

Figure 6. (A) Charge ratio within NPs (r_{NP}) and (B) percentage of SCX4 (◇) and D70Im54 (◆) included in NPs as a function of the mixing charge ratio n/p. [D70Im54] = 1 g L^{-1} and pH = 7

Figure 6A displays the variation of charge ratio n/p within the NPs (r_{NP}) upon increase of mixing charge ratio. The r_{NP} values were almost constant except in the case of the lowest amount of SCX4. An average value of 1.005 was obtained that indicates a stoichiometry in NPs close to charge compensation like in the case of NPs composed of SCXn and cationic surfactants (Wintgens, Harangozó, Miskolczy, Guigner, Amiel & Biczók, 2017; Wintgens et al., 2013). The fraction of the constituents incorporated in NPs substantially varied with the mixing ratio reaching a maximum around charge neutralization, when almost 99% of both SCX4 and dextran derivative molecules were incorporated in NPs (Figure 6B). The macromolecule–SCX4 associates were able to aggregate into NPs over a large mixing range. Their stoichiometry was close to the charge ratio, but their efficiency of formation attained maximum when the mixing charge ratio was close to 1.

3.4. Scheme of NPs formation

Because of its polyanionic character, SCXn can compact the chains of modified dextran by electrostatic interactions via the cationic moieties resulting in NP formation. Hydrogen bonding among polymer chains and also with SCXn probably contributes to the stability of the NPs. Dextrans with their flexible backbone may reach the optimal folding to accommodate around the calixarenes. Their persistence length (Rief, Fernandez & Gaub, 1998) of ~0.4 nm is lower than the calixarene diameters (1-2 nm). Scheme 2 rationalizes the association mechanism suggesting internal structure with microdomains corresponding to charge neutralization around the calixarene units. Depending on the mixing molar ratio, the positively charged spherical nanoparticles are stabilized by methylimidazolium groups on the surface, whereas the negatively charged ones are stabilized by an excess of SCXn. The spherical nanoassemblies with a diameter around 150 nm results from the association of numerous dextran chains and the worm-like appearance (as shown on cryo- TEM images)

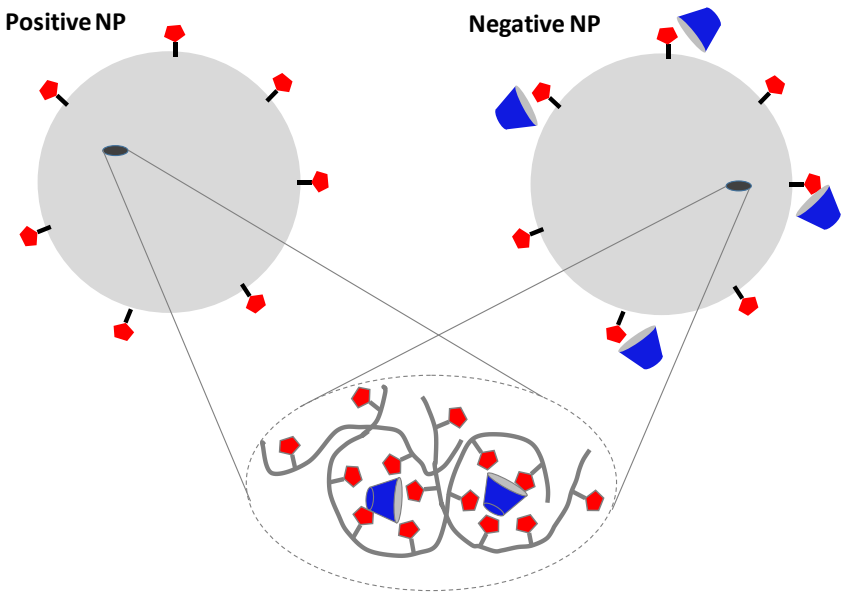

Scheme 2. Illustration of positively and negatively charged NPs formed between DxImy and SCX4

could be attributed to entanglement of polymer/SCXn microdomains. The experiments have established that NP sizes mainly depend on the total concentration and the imidazolium DS, but neither the cavity size nor the polymer molecular weight influences it.

Other cationic macromolecules such as protamine or chitosan have been reported to self-assemble with SCXn (Harangozó, Wintgens, Miskolczy, Amiel & Biczók, 2016; Peng, Wang, Guo & Liu, 2015; Wang, Guo, Zhao & Liu, 2016). It is worth comparing the properties of these NPs with those previously found for the product of SCXn self-organization with protonated chitosan (Harangozó, Wintgens, Miskolczy, Amiel & Biczók, 2016). The morphology of the NPs differed in the case of the two polysaccharides. DxImy assembled with SCXn to spherical nano-objects, whereas chitosan produced loose structures with irregular shape and somewhat larger size. The unlike appearance of the two types of associates may originate from the less flexible backbone of chitosan compared to dextran. Persistence length values of 9-12 nm were reported depending on the deacetylation degree of chitosan (Rinaudo, 2006). The semi-rigid character of chitosan chains may impede the

accommodation around SCXn. Therefore, the chitosan nanoparticles were less stable and were formed at much lower chitosan concentration (0.05 g L^{-1} compared to 1-2 g L^{-1} in this work).

3.5. Drug loading in the nanoparticles

SCXn can encapsulate alkaloids of pharmaceutical interest (Megyesi & Biczók, 2006, 2010; Yatsimirsky, 2012). Previous results demonstrated that these cavitands are capable of binding as many coralyne (Cor) molecules as the number of their 4-hydroxybenzenesulfonate units and the largest association efficiency is reached with SCX8 (Megyesi & Biczók, 2010). Hence, we used this alkaloid as a model compound to test whether dextran derivative–SCX8 NPs are able to entrap drug. D70Im54 or D500Im44 was mixed with Cor–SCX8 complex solutions at pH 7 keeping the polymer amount (1 g L^{-1}) constant. The total SCX8 concentration in the initial mixture ($[SCX8]_T$) was varied to change the mixing charge ratio n/p and to produce both positively and negatively charged NPs. (The positive charge of Cor was taken into account for n/p determination). The molar ratio of the total concentrations in the initial solutions ($[Cor]_T/[SCX8]_T$) was around 0.5. Although Cor and SCX8 can form complexes with stoichiometry as high as 8 NPs were destabilized by Cor confinement and large aggregates were produced when $[Cor]_T/[SCX8]_T$ exceeded 1. To determine the fraction of Cor embedded in NPs, the suspensions were ultracentrifuged and the concentration of alkaloid in the supernatant ($[Cor]_S$) was determined by spectrophotometric measurements monitoring its absorbance at 423 nm. The association efficiency (*AE*) and the loading capacity (*LC*) of NPs were calculated as follows:

$$AE = \frac{[\mathrm{Cor}]_\mathrm{T} - [\mathrm{Cor}]_\mathrm{S}}{[\mathrm{Cor}]_\mathrm{T}} \times 100 \quad (1)$$

$$LC = \frac{[\mathrm{Cor}]_\mathrm{T} - [\mathrm{Cor}]_\mathrm{S}}{[\mathrm{SCX8}]_\mathrm{T} + [\mathrm{Dext}]_\mathrm{T}} \times 100 \quad (2)$$

where $[Cor]_T$, $[SCX8]_T$, and $[Dext]_T$ represent the total concentrations of Cor, SCX8, and dextran derivatives, respectively. Table 2 summarizes the variation of the NP characteristics with the concentrations of the constituents in the starting mixtures at pH 7. Efficient Cor confinement was achieved, which insignificantly changed the size and stability of the prepared NPs at $([Cor]_T/[SCX8]_T) \approx 0.5$. The AE and LC values were similar for both positively and negatively charged aggregates alike suggesting that alkaloid binding occurs not on the surface but inside the NPs. The affinity of Cor was slightly higher to the particles comprising D70Im54 instead of D500Im44. For the former dextran derivative, almost quantitative Cor encapsulation could be reached.

Table 2. SCX8 concentration, mixing charge ratio n/p and $[Cor]_T/[SCX8]_T$ molar ratio used for the preparation of NPs at 1 g L^{-1} modified dextran concentration and pH 7. Association efficiency (AE), loading capacity (LC), zeta potential (ζ), mean diameter (d), and polydispersity index (PDI) of the NPs

	$[SCX8]_T$ (mM)	Mixing charge ratio n/p	Molar ratio $[Cor]_T/[SCX8]_T$[a]	AE (%)	LC (weight %)	ζ (mV)	d (nm)	PDI
D70Im54	0.178	0.88	0.51	92.6	2.5	[b]	174	0.10
	0.188	0.93	0.50	97.2	2.7	+17.0	210	0.11
	0.199	0.98	0.50	99.1	2.9	-16.1	189	0.06
	0.210	1.03	0.49	96.3	2.9	[b]	159	0.16
D500Im44	0.144	0.82	0.46	88.4	1.9	[b]	180	0.08
	0.155	0.88	0.47	93.1	2.1	+19.1	177	0.11
	0.177	1.01	0.47	95.8	2.4	-21.5	162	0.14
	0.188	1.06	0.48	84.9	2.3	[b]	160	0.17

[a] molar ratio of the total Cor and SCX8 concentrations in the initial mixture, [b] not determined

The presence of SCXn allows the encapsulation of alkaloids such as coralyne in the NPs. Our previous study with chitosan showed that it was possible to load as much as 4.5 Cor per SCX8. In this work, the maximum loading is 0.5 Cor per SCX8 was reached. NPs were destabilized in the presence of more Cor. The association between SCX8 and the modified dextran is less cooperative when the negative charges of SCX8 are partly neutralized by Cor. Despite the lower LC in DxImy–SCX8 NPs than in chitosan–SCX8 NPs, the total amount of encapsulated Cor is at least twice as high in the former case because larger NP concentration can be attained due to the more substantial solubility of DxImy. Another advantage of methylimidazolium-conjugated dextrans is that they readily produce NPs with SCX8 even at pH 7 where the application of chitosan is hindered by its low solubility. It is beneficial that narrower NP size distribution can be obtained when DxImy polymer is applied instead of protonated chitosan and both positively and negatively charged NPs can incorporate drugs.

4. Conclusions

SCXn polyanionic macrocycles not only induce self-assembly with methylimidazolium-conjugated dextrans into NPs by supramolecular crosslinking of the polymer chains but also can serve as molecular containers within NPs to encapsulate the biomedically important coralyne alkaloid. Despite its cationic character, similar amount of coralyne can be confined in both positively and negatively charged NPs because of the large binding affinity of the alkaloid to the SCXn constituents. The hydrophilic and flexible backbone of dextran polycations is advantageous for the association with SCXn into stable spherical aggregates. The molecular mass of DxImy polymers and the size of the SCXn constituent barely influence the properties of the self-organized NPs, but the low degree of substitution with methylimidazolium moieties on the dextran backbone exerts unfavorable effect.

Acknowledgements

This work was supported by the BIONANO GINOP-2.3.2-15-2016-00017 project and the National Research, Development and Innovation Office Grant K123995 to ZM and LB.

Appendix A. Supplementary data

Supplementary material related to this article can be found, in the online version, at doi:https://doi.org/

References

Bai, G., Nichifor, M., Lopes, A., & Bastos, M. (2005). Thermodynamic characterization of the interaction behavior of a hydrophobically modified polyelectrolyte and oppositely charged surfactants in aqueous solution: Effect of surfactant alkyl chain length. *Journal of Physical Chemistry B, 109*(1), 518-525.

Bhattacharyya, R., Gupta, P., Bandyopadhyay, S. K., Patro, B. S., & Chattopadhyay, S. (2018). Coralyne, a protoberberine alkaloid, causes robust photosenstization of cancer cells through atr-p38 mapk-bax and jak2-stat1-bax pathways. *Chemico-Biological Interactions, 285*, 27-39.

Bhattacharyya, R., Saha, B., Tyagi, M., Bandyopadhyay, S. K., Patro, B. S., & Chattopadhyay, S. (2017). Differential modes of photosensitisation in cancer cells by berberine and coralyne. *Free Radical Research, 51*(7-8), 723-738.

Cheow, W. S., & Hadinoto, K. (2012). Self-assembled amorphous drug–polyelectrolyte nanoparticle complex with enhanced dissolution rate and saturation solubility. *Journal of Colloid and Interface Science, 367*(1), 518-526.

Chyan, W., Kilgore, H. R., & Raines, R. T. (2018). Cytosolic uptake of large monofunctionalized dextrans. *Bioconjugate Chemistry*, *29*(6), 1942-1949.

Gatto, B., Sanders, M. M., Yu, C., Wu, H.-Y., Makhey, D., LaVoie, E. J., & Liu, L. F. (1996). Identification of topoisomerase i as the cytotoxic target of the protoberberine alkaloid coralyne. *Cancer Research, 56*(12), 2795-2800.

Ghimici, L., & Nichifor, M. (2018). Flocculation characteristics of a biodegradable polymer based on dextran. *Separation and Purification Technology, 194*, 48-55.

Giri, T. K., & Ghosh, B. (2018). *Polysaccharide based nano-biocarrier in drug delivery*. CRC Press

Harangozó, J. G., Wintgens, V., Miskolczy, Z., Amiel, C., & Biczók, L. (2016). Nanoparticle formation of chitosan induced by 4-sulfonatocalixarenes: Utilization for alkaloid encapsulation. *Colloid and Polymer Science, 294*(11), 1807-1814.

Heinze, T., Liebert, T., Heublein, B., & Hornig, S. (2006). Functional polymers based on dextran. In D. Klemm (Ed.). *Polysaccharides ii* (pp. 199-291). Berlin, Heidelberg: Springer Berlin Heidelberg.

Hosseinkhani, H., Azzam, T., Tabata, Y., & Domb, A. J. (2004). Dextran–spermine polycation: An efficient nonviral vector for in vitro and in vivo gene transfection. *Gene Therapy, 11*, 194.

Huang, G., & Huang, H. (2018). Application of dextran as nanoscale drug carriers. *Nanomedicine, 13*(24), 3149-3158.

Jafarzadeh-Holagh, S., Hashemi-Najafabadi, S., Shaki, H., & Vasheghani-Farahani, E. (2018). Self-assembled and ph-sensitive mixed micelles as an intracellular doxorubicin delivery system. *Journal of Colloid and Interface Science, 523*, 179-190.

Jin, R., Guo, X., Dong, L., Xie, E., & Cao, A. (2017). Amphipathic dextran-doxorubicin prodrug micelles for solid tumor therapy. *Colloids and Surfaces B: Biointerfaces, 158*, 47-56.

Kumari, S., Badana, A. K., Mohan, G. M., Shailender Naik, G., & Malla, R. (2017). Synergistic effects of coralyne and paclitaxel on cell migration and proliferation of breast cancer cells lines. *Biomedicine and Pharmacotherapy 91*, 436-445.

Maia, J., Evangelista, M. B., Gil, H., & Ferreira, L. (2014). Dextran-based materials for biomedical applications. In M. H. Gil (Ed.). *Carbohydrates applications in medicine* (pp. 31-54). Irvine, CA, USA: Research Signpost.

Megyesi, M., & Biczók, L. (2006). Considerable fluorescence enhancement upon supramolecular complex formation between berberine and p-sulfonated calixarenes. *Chemical Physics Letters, 424*(1-3), 71-76.

Megyesi, M., & Biczók, L. (2010). Considerable change of fluorescence properties upon multiple binding of coralyne to 4-sulfonatocalixarenes. *Journal of Physical Chemistry B, 114*(8), 2814-2819.

Megyesi, M., Biczók, L., & Görner, H. (2009). Dimer-promoted fluorescence quenching of coralyne by binding to anionic polysaccharides. *Photochemical and Photobiological Sciences, 8*(4), 556-561.

Mehvar, R. (2000). Dextrans for targeted and sustained delivery of therapeutic and imaging agents. *Journal of Controlled Release, 69*(1), 1-25.

Myrick James, M., Vendra Venkat, K., & Krishnan, S. (2014). Self-assembled polysaccharide nanostructures for controlled-release applications. *Nanotechnology Reviews* (Vol. 3, p. 319).

Nichifor, M., Lopes, S., Bastos, M., & Lopes, A. (2004). Self-aggregation of amphiphilic cationic polyelectrolytes based on polysaccharides. *Journal of Physical Chemistry B, 108*(42), 16463-16472.

Nichifor, M., Stanciu, M. C., & Simionescu, B. C. (2010). New cationic hydrophilic and amphiphilic polysaccharides synthesized by one pot procedure. *Carbohydrate Polymers, 82*(3), 965-975.

Pawar, R., Jadhav, W., Bhusare, S., Borade, R., Farber, S., Itzkowitz, D., & Domb, A. (2008). Polysaccharides as carriers of bioactive agents for medical applications. In R. L. Reis, N. M. Neves, J. F. Mano, M. E. Gomes, A. P. Marques & H. S. Azevedo (Eds.). *Natural-based polymers for biomedical applications* (pp. 3-53): Woodhead Publishing.

Peng, S., Wang, K., Guo, D.-S., & Liu, Y. (2015). Supramolecular polymeric vesicles formed by p-sulfonatocalix[4]arene and chitosan with multistimuli responses. *Soft Matter, 11*(2), 290-296.

Persson, B., Hugerth, A., Caram-Lelham, N., & Sundelöf, L. O. (2000). Dextran sulfate−amphiphile interaction; effect of polyelectrolyte charge density and amphiphile hydrophobicity. *Langmuir, 16*(2), 313-317.

Prado, H. J., & Matulewicz, M. C. (2014). Cationization of polysaccharides: A path to greener derivatives with many industrial applications. *European Polymer Journal, 52*, 53-75.

Rief, M., Fernandez, J. M., & Gaub, H. E. (1998). Elastically coupled two-level systems as a model for biopolymer extensibility. *Physical Review Letters, 81*(21), 4764-4767.

Rinaudo, M. (2006). Chitin and chitosan: Properties and applications. *Progress in Polymer Science, 31*(7), 603-632.

Son, S., Rao, N. V., Ko, H., Shin, S., Jeon, J., Han, H. S., Nguyen, V. Q., Thambi, T., Suh, Y. D., & Park, J. H. (2018). Carboxymethyl dextran-based hypoxia-responsive

nanoparticles for doxorubicin delivery. *International Journal of Biological Macromolecules, 110*, 399-405.

Suga, K., Ohzono, T., Negishi, M., Deuchi, K., & Morita, Y. (1998). Effect of various cations on the acidity of p-sulfonatocalixarenes. *Supramolecular Science, 5*(1-2), 9-14.

Tang, Y., Li, Y., Xu, R., Li, S., Hu, H., Xiao, C., Wu, H., Zhu, L., Ming, J., Chu, Z., Xu, H., Yang, X., & Li, Z. (2018). Self-assembly of folic acid dextran conjugates for cancer chemotherapy. *Nanoscale, 10*(36), 17265-17274.

Thomas, J. J., Rekha, M. R., & Sharma, C. P. (2012). Unraveling the intracellular efficacy of dextran-histidine polycation as an efficient nonviral gene delivery system. *Molecular Pharmaceutics, 9*(1), 121-134.

Tseng, W.-C., & Jong, C.-M. (2003). Improved stability of polycationic vector by dextran-grafted branched polyethylenimine. *Biomacromolecules, 4*(5), 1277-1284.

Wang, K., Guo, D.-S., Zhao, M.-Y., & Liu, Y. (2016). A supramolecular vesicle based on the complexation of p-sulfonatocalixarene with protamine and its trypsin-triggered controllable-release properties. *Chemistry – A European Journal, 22*(4), 1475-1483.

Wintgens, V., Biczók, L., & Miskolczy, Z. (2011). Thermodynamics of host-guest complexation between p-sulfonatocalixarenes and 1-alkyl-3-methylimidazolium type ionic liquids. *Thermochimica Acta, 523*(1-2), 227-231.

Wintgens, V., Harangozó, J. G., Miskolczy, Z., Guigner, J.-M., Amiel, C., & Biczók, L. (2017). Effect of headgroup variation on the self-assembly of cationic surfactants with sulfonatocalix[6]arene. *Langmuir, 33*(32), 8052-8061.

Wintgens, V., Layre, A.-M., Hourdet, D., & Amiel, C. (2012). Cyclodextrin polymer nanoassemblies: Strategies for stability improvement. *Biomacromolecules, 13*(2), 528-534.

Wintgens, V., Le Coeur, C., Amiel, C., Guigner, J. M., Harangozó, J. G., Miskolczy, Z., & Biczók, L. (2013). 4-sulfonatocalix[6]arene-induced aggregation of ionic liquids. *Langmuir, 29*(25), 7682-7688.

Yatsimirsky, A. K. (2012). Host-guest chemistry of alkaloids. *Natural Product Communications, 7*(3), 369-380.

Zheng, Y., Monty, J., & Linhardt, R. J. (2015). Polysaccharide-based nanocomposites and their applications. *Carbohydrate Research, 405*, 23-32.